Dielectronic recombination processes through doubly excited states ($4l4l'$, $4l5l'$) in Co-like Pd ions

Hong Zhang, Yueming Li, Jun Yan, and Jianguo Wang
The Key Laboratory of Computational Mathematics, Institute of Applied Physics and Computational Mathematics, Beijing 100088, People's Republic of China
(Received 28 October 2004; published 11 April 2005)

Ab initio calculations of dielectronic recombination processes from the ground state [Ne *core*]$3s^23p^63d^9$ of Co-like Pd^{19+} ion through doubly excited states [Ne *core*]$3s^23p^63d^84lnl'$, [Ne *core*]$3s^23p^53d^94lnl'$, and [Ne *core*]$3s3p^63d^94lnl'$ ($n=4$ or 5) of Ni-like Pd^{18+} ions are performed using the multiconfiguration Hartree-Fock method with relativistic correction. Total and state-to-state rate coefficients are obtained in the temperature range from 0.1 to 10^4 eV. Comparison of the rate coefficients from 3*s*, 3*p*, and 3*d* subshell excitations shows 3*d* subshell excitation dominates over the others in the whole energy region, but 3*p* and 3*s* subshell excitation cannot be neglected in high temperature; when electron temperature $T>500$ eV, the contributions from 3*p* and 3*s* subshells are more than 40% and 10% of the dielectronic recombination (DR) rate coefficients from 3*d* subshell excitations; especially for the DR processes through the doubly excited states $n=5$, the contribution from 3*p* subshell excitations is approximately 60% of the rate coefficients from 3*d* subshell excitations. The two-electron radiative transitions, such as $3d^84p4d\rightarrow 3d^94s$ and $3d^84d^2\rightarrow 3d^94p$, are found to be important due to the strong configuration interactions, which contribute more than 10% of the total rate coefficients through the doubly excited states [Ne *core*]$3s^23p^63d^84l4l'$.

DOI: 10.1103/PhysRevA.71.042705 PACS number(s): 34.80.Kw, 34.80.Lx

I. INTRODUCTION

Dielectronic recombination (DR) can be regarded as a resonant radiative recombination process. As a free electron with a specific kinetic energy collides with an ion A^{q+}, one of the bound electrons of A^{q+} is excited from the initial n_il_i orbital into the n_fl_f orbital. The free electron is then captured into an unoccupied orbital *nl* and forms a resonant doubly excited state; subsequently, the resonant doubly excited state decays into a nonautoionizing state through radiative transition processes. Its importance influencing the ionic balance in high-temperature plasma, such as a solar corona, has been known for many years [1]. Its radiative emission is a significant contributor to plasma cooling in hot plasmas in fusion experiments. The dielectronic satellites of hydrogenlike ions have also been used to diagnose plasma densities in high-density plasmas [2] and the electron temperatures in solar flares [3]. In addition to its applications in astrophysics and fusion plasmas, DR process is of importance for studies of the structure and decay dynamics of atomic doubly excited states [4].

A number of experimental and theoretical works on DR processes exist; most of them focus on *K*-shell or *L*-shell ions, and few of them study the *M*-shell ions, because the complicated structures with 3 or 4 open shells and strong configuration interactions are often involved in *M*-shell DR processes [5–9]. However, *M*-shell DR processes play an important role in many applications. In the theoretical simulation of Ni-like x-ray laser, Co-like DR processes can populate the high-energy levels of x ray and affect the x-ray amplification and x-ray transfer [10–12]. In the indirect inertial confinement fusion, DR processes can decrease the average ionization degree by recombining, and decrease plasma temperature by emitting photons, directly affecting the Au *M*-band spectra and x-ray transforming efficiencies [13–16]. So, both experimental and theoretical data on DR processes of *M*-shell ions are required.

In this paper, using the multiconfiguration Hartree-Fock method with relativistic correction [17], we consider the DR of a Co-like Pd^{19+} in its ground state [Ne *core*]$3s^23p^63d^9$, through the doubly excited states of Ni-like Pd^{18+} ions [Ne *core*]$3s^23p^63d^84lnl'$, [Ne *core*]$3s^23p^53d^94lnl'$, [Ne *core*]$3s3p^63d^94lnl'$ ($n=4$ or 5), where [Ne core] denotes the full $1s^22s^22p^6$ electronic inner shells. There are many DR channels, which can be expressed as

$$\begin{aligned} &Pd^{19+}([\text{Ne } core]3s^23p^63d^9)+e \\ &\quad\rightarrow \begin{cases} Pd^{18+}([\text{Ne } core]3s^23p^63d^84lnl')^{**} \\ Pd^{18+}([\text{Ne } core]3s^23p^53d^94lnl')^{**} \\ Pd^{18+}([\text{Ne } core]3s3p^63d^94lnl')^{**} \end{cases} \\ &\quad\rightarrow \begin{cases} Pd^{18+}([\text{Ne } core]3s^23p^63d^9n''l'')^{*} \\ Pd^{18+}([\text{Ne } core]3s^23p^53d^9n''l'')^{*} \\ Pd^{18+}([\text{Ne } core]3s3p^63d^{10}n''l'')^{*} \\ Pd^{18+}([\text{Ne } core]3s^23p^63d^{10})^{*}. \end{cases} \end{aligned} \tag{1}$$

Here, $n''=4$ or 5; the three intermediate doubly excited states correspond to 3*s*, 3*p*, 3*d* subshell excitations, respectively. We calculate both total and state-to-state DR rate coefficients, compare the rate coefficients from 3*s*, 3*p*, 3*d* subshell excitations, and discuss the effects of two-electron radiative transitions and configuration interactions in *M*-shell DR processes.

II. THEORETICAL METHODS

In the isolated-resonance approximation, the DR cross sections from initial state *i* into a final state *f* through an

intermediate doubly excited state d is written as (atomic units are used throughout unless specified) [18]

$$\sigma_{idf} = \frac{\pi^2\hbar^3}{m_e\varepsilon_{id}}\frac{g_d}{2g_i}\frac{A^a_{di}\cdot A^r_{df}}{\sum_{f'}A^r_{df'}+\sum_{i'}A^a_{di'}}\delta(\varepsilon-\varepsilon_{id}), \qquad (2)$$

where m_e is mass of electron, ε_{id} is resonance energy, and also Auger electron energy, g_i and g_d are the statistical weight of the states i and d, respectively. A^a_{di} is the Auger decay rate, which can be calculated by Fermi's golden rule

$$A^a_{di} = \frac{2\pi}{\hbar}\left|\left\langle\Psi_d\left|\sum_{s<t}\frac{1}{r_{s,t}}\right|\Psi_{i\varepsilon_{id}}\right\rangle\right|^2, \qquad (3)$$

where Ψ_d and $\Psi_{i\varepsilon_{id}}$ are atomic wave functions for the d state and i state plus a free electron. A^r_{df} is radiative decay rate, which can be defined as

$$A^r_{df} = \frac{4e^2\omega}{3\hbar c^3 g_d}|\langle\Psi_d|T^{(1)}|\Psi_f\rangle|^2, \qquad (4)$$

where ω is photon energy and $T^{(1)}$ is electronic dipole operator, Ψ_f is the atomic wave function for the final state f. Ψ_f is the linear combination of the configuration wave functions $\Phi(\Gamma_\lambda)$, with mixing coefficients between different configurations. $\Phi(\Gamma_\lambda)$ are constituted as antisymmetrized product-type wave functions from central-field Hartree-Fock orbitals with appropriate angular momentum coupling. Ψ_d is constructed the same as Ψ_f.

The DR strengths, which are the integral of the DR cross section over the natural width of the resonance, can be written as

$$S_{id} = \frac{\pi^2\hbar^3}{m_e\varepsilon_{id}}\frac{g_d}{2g_i}\frac{A^a_{di}\sum_f A^r_{df}}{\sum_{f'}A^r_{df'}+\sum_{i'}A^a_{di'}}. \qquad (5)$$

We assume the velocity distribution of the free electron as the Maxwell-Boltzmann distribution; then, the DR rate coefficients can be expressed as [18]

$$\alpha^{DR}_{idf} = \left(\frac{2\pi\hbar^2}{m_e\kappa T_e}\right)^{3/2}\frac{g_d}{2g_i}\exp\left(-\frac{\varepsilon_{id}}{\kappa T_e}\right)\frac{A^a_{di}A^r_{df}}{\sum_{f'}A^r_{df'}+\sum_{i'}A^a_{di'}}. \qquad (6)$$

Here, T_e is the electron temperature and κ is the Boltzmann constant.

III. RESULTS AND DISCUSSIONS

Using the multiconfiguration Hartree-Fock method with relativistic correction [17], we calculate the DR of a Co-like Pd^{19+} in its ground state [Ne *core*]$3s^23p^63d^9$, through a Ni-like Pd^{18+} [Ne *core*]$3s^23p^63d^84lnl'$, [Ne *core*]$3s^23p^53d^94lnl'$, [Ne *core*]$3s3p^63d^94lnl'$. There are 92 intermediate configurations and more than 10 000 detailed levels included in the calculations. The ground state [Ne *core*]$3s^23p^63d^9$ of Co-like Pd^{19+} includes two levels with total angular momentum $j=3/2$ and $5/2$. After finishing the separate calculations on DR rate coefficients for the two levels, we obtain the DR rate coefficients by averaging the two separate rate coefficients by statistical weight of the two total angular momenta. Besides the level-to-level rate coefficients, we can obtain the configuration-averaged and total DR rate coefficients by averaging on initial states and summations on final states.

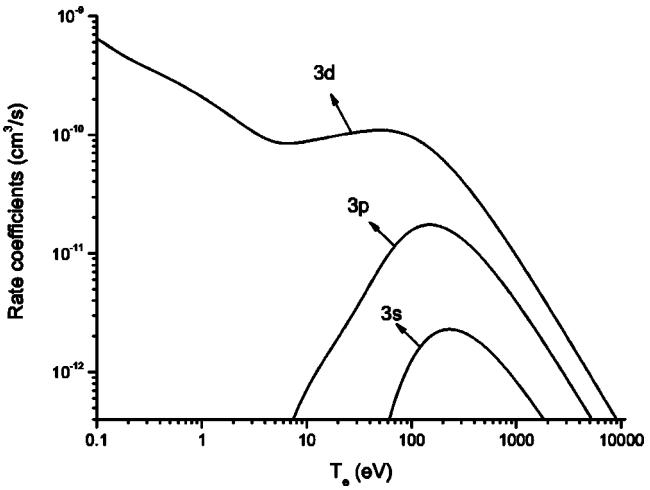

FIG. 1. Total rate coefficient as a function of electron temperature for DR processes through doubly excited states Pd^{18+} [Ne *core*]$3s^23p^63d^84l4l'$, $3s^23p^53d^94l4l'$, $3s3p^63d^94l4l'$, and the curves corresponding to $3d$, $3p$, and $3s$ subshell excitations.

A. Total DR rate coeffcients

The total DR rate coefficients through doubly excited states Pd^{18+} [Ne *core*]$3s^23p^63d^84lnl'$, $3s^23p^53d^94l4l'$, $3s3p^63d^94l4l'$ are plotted in Fig. 1, and different curves correspond to the $3d$, $3p$, and $3s$ subshell excitations. The DR rate coefficients from $3d$ subshell excitation increase with the decreasing electron temperature in the low temperature and reach 6.2×10^{-10} cm^3/s at the calculated lowest temperature 0.1 eV, which is different from the K-shell DR processes [19] and similar to the $\Delta n=0$ L-shell DR processes [20]. As a function of the electron temperature, the DR rate coefficients depend mainly on $T_e^{-3/2}$ and $\exp(-\varepsilon_{id}/T_e)$ in Eq. (6), i.e., they are determined by ε_{id}.

In the doubly excited state of Pd^{18+} $3d^84p4d$, there exist some levels just above the autoionization threshold which means the free-electron energy ε_{id} is close to zero; we will discuss this in more detail in Sec. III B. It can be easily understood from Eq. (6) that it is these states that strongly enhance and even dominate the whole DR process at low electron temperature for M-shell ions. It should be stressed that such peculiar levels are of special interest in the research of x-ray lasers, since the strong capture to particular autoionization states may lead to a population inversion and a lasing process [8].

In the temperature range from 5 to 100 eV, there exists a platform; then, the DR rate coefficients drop quickly with increasing temperature. The DR rate coefficients from $3p$ and $3s$ subshells increase with temperature, reach a maximum at approximately 200–300 eV, and then decrease

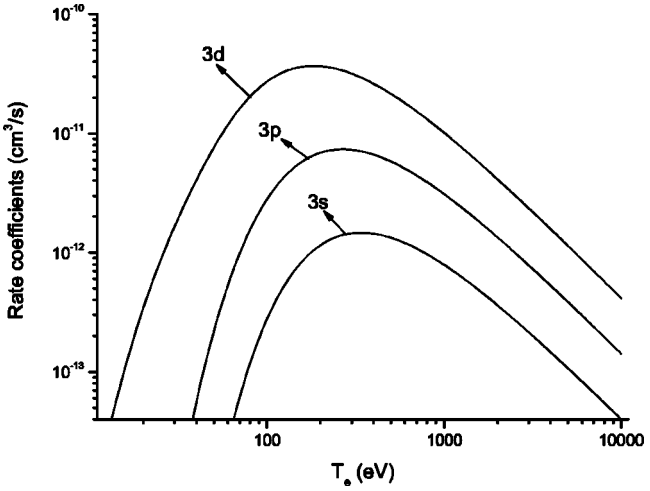

FIG. 2. Total rate coefficient as a function of electron temperature for DR processes through doubly excited states Pd^{18+} [Ne *core*]$3s^23p^63d^84l5l'$, $3s^23p^53d^94l5l'$, $3s3p^63d^94l5l'$, and the curves corresponding to 3*d*, 3*p*, and 3*s* subshell excitations.

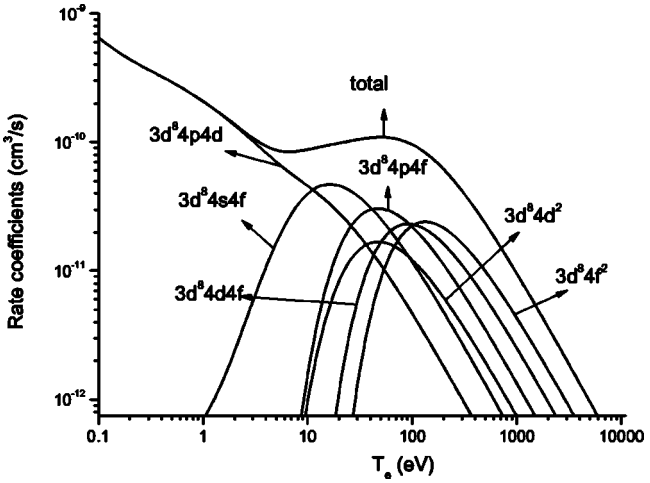

FIG. 3. Rate coefficient as a function of electron temperature for DR processes through the different doubly excited states Pd^{18+} [Ne *core*]$3s^23p^63d^84l4l'$.

quickly. When electron temperature $T_e<10$ eV, the DR rate coefficients from 3*d* subshells are 2–4 magnitudes larger than that from 3*p* and 3*s* subshells. With the increasing electron temperature, the contributions from 3*p* and 3*s* subshells gradually become larger; when $T_e>500$ eV, the rate coefficients from 3*p* and 3*s* subshells are more than 40% and 10% of that from 3*d* subshells. So, the DR rate coefficients from 3*p* and 3*s* subshells cannot be neglected in the higher electron temperature.

The total DR rate coefficients through doubly excited states Pd^{18+} [Ne *core*]$3s^23p^63d^84l5l'$, $3s^23p^53d^94l5l'$, $3s3p^63d^94l5l'$ are shown in Fig. 2. Because the energies of doubly excited states are more than 100 eV beyond the autoionization threshold, the rate coefficients from 3*d*, 3*p*, and 3*s* subshells all behave as single peaks at about 200–500 eV. The peak positions of 3*p* and 3*s* move to higher energies than that of 3*d*, since the energies of the doubly excited states from 3*p* and 3*s* subshell excitations are higher than that of 3*d*. Although the DR process from 3*d* subshells still dominates over the 3*p* and 3*s* subshells, the DR rate coefficients from 3*p* subshells approach that from 3*d* when electron temperature $T_e>800$ eV, while the DR rate coefficients from 3*s* subshells are approximately 10% of that from 3*d* subshells. So, the contributions from 3*p* and 3*s* subshell excitations cannot be neglected for the DR processes through doubly excited states $4l5l'$ as well as doubly excited states $4l4l'$.

Comparing Fig. 2 with Fig. 1, the peak of rate coefficients through doubly excited states $4l5l'$ is approximately 40% of that through doubly excited states $4l4l'$ at about 100 eV. Based on n^{-3} scaling law of rate coefficients [20–22], the maximum of rate coefficients from $4l5l'$ should be approximately 50% of that from $4l4l'$, which is larger than the present value. The reason may be that the n^{-3} scaling law of rate coefficients is not available for the present doubly excited states with lower principal quantum number $n=4$ and 5. We will test the scaling law of rate coefficients in the future when we carry out calculations for the higher doubly excited states $4lnl'(n\geqslant 6)$, and also check the validity of scaling law for radiative and Auger decay rates [20].

B. State-to-state DR rate coefficients

In order to simplify the discussion, the configuration-to-configuration DR rate coefficients are calculated by averaging for initial states and summation for final states on level-to-level (in LS couplings [17]) rate coefficients, and in the following, the state-to-state rate coefficients represent the configuration-to-configuration DR rate coefficients. The level-to-level DR rate coefficients are available by request or by visiting our database (http://www.camdb.ac.cn).

Figure 3 plots the DR rate coefficients through the different intermediate doubly excited states of Pd^{18+} [Ne *core*]$3s^23p^63d^84l4l'$, and the final states of radiative stabilizations are summed. In the lower energy range, the DR processes through the doubly excited states Pd^{18+} [Ne *core*]$3s^23p^63d^84p4d$ dominate over others. There are many levels in the configuration of Pd^{18+} [Ne *core*]$3s^23p^63d^84p4d$; some of them are beyond the autoionization threshold and some of them are below the threshold. These levels come close to the autoionization threshold decay by emitting the Auger electron with very low energy, and in the inverse processes, it means the free-electron energies ε_{id} in dielectronic capture processes are very low. As we discussed in Sec. III A and based on Eq. (6), the large rate coefficients at lower temperature come from the DR processes through these doubly excited states with energies close to the autoionization threshold. Meanwhile, based on Eq. (2) and Eq. (5), the DR cross sections and DR strengths are inversely proportional to the free-electron energies ε_{id}, so the cross sections and collision strengths are also the largest at lower electron energies, which is similar to the $\Delta n=0$ *L*-shell DR processes [20]. In Table I, we present the part energies of resonance electron (Auger electron), radiative decay rates, Auger rates, and DR strengths through doubly excited states Pd^{18+} [Ne *core*]$3s^23p^63d^84p4d$ with the total angular momentum of $J=0-6$; it should be noted that only a

TABLE I. Energies of resonance electrons, radiative decay rates, Auger rates, and DR strengths through doubly excited states of Ni-like Pd^{18+} [Ne *core*]$3s^23p^63d^84p4d$, and the total angular momentum $J=0-6$. Here, the initial state of the DR process is Pd^{19+} [Ne *core*]$3s^23p^63d^9$ ($j=5/2$). For $J=1-5$, only a few of the lowest resonance energy levels are listed.

Total J	$\varepsilon_{\mathrm{id}}$ (eV)	A^r (s^{-1})	A^a (s^{-1})	S_{id} (10^{-20} cm^2/eV)
$J=0$	0.601	7.17×10^{10}	3.85×10^{11}	4.15
	4.039	1.00×10^{11}	2.08×10^{11}	0.69
	5.408	9.28×10^{10}	7.00×10^{9}	0.05
	14.358	1.04×10^{11}	5.85×10^{13}	0.03
	20.571	2.78×10^{12}	4.17×10^{14}	5.54
$J=1$	0.217	1.89×10^{11}	6.59×10^{11}	83.76
	0.700	2.89×10^{11}	2.70×10^{11}	24.68
	1.282	2.67×10^{11}	3.83×10^{11}	15.19
	1.751	3.32×10^{11}	5.42×10^{11}	14.55
	3.120	2.17×10^{11}	2.58×10^{11}	4.67
$J=2$	0.054	1.51×10^{11}	1.29×10^{12}	516.43
	0.364	1.89×10^{11}	2.05×10^{12}	98.07
	0.737	2.14×10^{11}	3.97×10^{12}	56.83
	1.091	1.91×10^{11}	4.20×10^{11}	24.82
	1.701	1.92×10^{11}	9.60×10^{10}	7.76
	1.948	7.24×10^{10}	1.02×10^{11}	4.48
$J=3$	0.569	1.53×10^{11}	1.46×10^{12}	70.27
	0.711	2.55×10^{11}	5.50×10^{11}	70.76
	0.790	2.26×10^{11}	9.31×10^{11}	66.47
	1.374	1.68×10^{11}	7.90×10^{11}	11.29
	1.660	1.74×10^{11}	1.84×10^{12}	27.66
	1.910	9.59×10^{10}	1.84×10^{11}	9.53
$J=4$	0.073	7.20×10^{10}	9.93×10^{11}	341.41
	0.481	1.91×10^{11}	1.57×10^{12}	131.41
	0.655	2.09×10^{11}	5.77×10^{11}	86.96
	0.940	1.97×10^{11}	3.18×10^{12}	73.26
	1.668	1.52×10^{11}	1.09×10^{11}	14.13
$J=5$	0.301	7.86×10^{10}	3.74×10^{11}	97.91
	0.637	2.96×10^{10}	1.79×10^{11}	18.09
	2.334	2.11×10^{11}	5.00×10^{9}	0.95
	3.401	5.83×10^{10}	1.20×10^{10}	1.33
	4.038	9.71×10^{10}	2.70×10^{10}	2.37
$J=6$	0.284	2.19×10^{10}	4.00×10^{9}	6.39
	1.589	7.10×10^{10}	1.30×10^{10}	3.71
	4.770	3.79×10^{10}	1.90×10^{10}	1.42

few of the lowest resonance energy levels are listed for $J=1-5$. The levels with the lower resonance energies have the larger DR strengths; the reason is that the DR strengths are inversely proportional to the resonance electron energies ε_{id}, and not because the levels have larger radiative and Auger decay rates, as shown in Table I. The lowest resonance energy is 0.054 eV in $J=2$, and corresponding DR strength

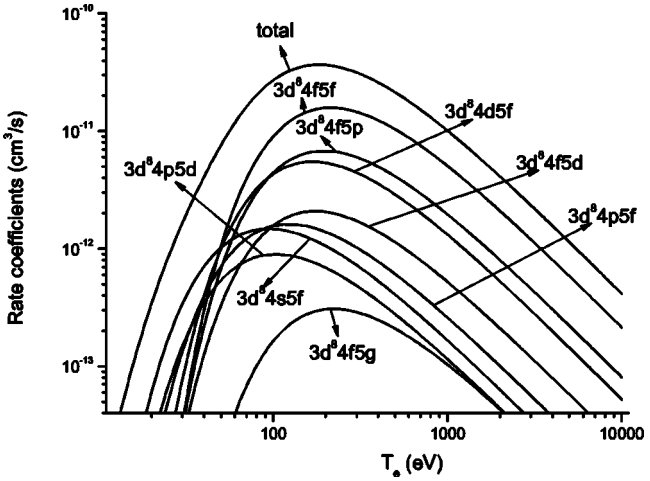

FIG. 4. Rate coefficient as a function of electron temperature for DR processes through the different doubly excited states Pd^{18+} [Ne *core*]$3s^23p^63d^84l5l'$.

516.43×10^{-20} cm^2/eV is the largest. It can be expected that one peak of the DR rate coefficients exists at temperature $\sim$0.054 eV, which will induce the increasing DR rate coefficients as the temperature decrease in the calculated temperature range.

In the higher temperature, the contributions from Pd^{18+} [Ne *core*]$3s^23p^63d^84s4f$, $3d^84p4f$, $3d^84d4f$, $3d^84d^2$, and $3d^84f^2$ increase gradually, and their peak positions depend on their energies. The summation of these rate coefficients form a platform between 7–100 eV, and one peak at about 60 eV. There are no contributions from Pd^{18+} [Ne *core*]$3s^23p^63d^84s^2$, $3d^84s4p$, $3d^84s4d$, and $3d^84p^2$ because the energies of these doubly excited states are below autoionization thresholds. For the ions in an isoelectronic sequence, the number of doubly excited states below the autoionization threshold increases as the nuclear charge increases [5]. It is expected in the present isoelectronic sequence that all the energies of doubly excited states of Pd^{18+} [Ne *core*]$3s^23p^63d^84l4l'$ will be lower than the ionization threshold when the nuclear charge increases to a definite value, and then DR processes cannot occur through the doubly excited states Pd^{18+} [Ne *core*]$3s^23p^63d^84l4l'$.

The DR rate coefficients from different doubly excited states Pd^{18+} [Ne *core*]$3s^23p^63d^84l5l'$ are plotted in Fig. 4. It should be noted that some smaller DR rate coefficients, such as through doubly excited states Pd^{18+} [Ne *core*]$3s^23p^63d^84s5p$ and $3d^84p5s$, are not plotted in the figure. Each doubly excited state corresponds to one peak of the DR rate coefficients, and the position of the peak is determined by the energies of the doubly excited energies. The contributions from doubly excited states Pd^{18+} [Ne *core*]$3s^23p^63d^84p5l$ are located in the lower energy region, and Pd^{18+} [Ne *core*]$3s^23p^63d^84f5l$ contributes in the higher energy region. The main contribution comes from the doubly excited states including the orbitals of nf and np, because the radiative decay rates of nf, np-$3d$ are larger than others, and furthermore, contribution from the doubly excited states including nf is larger than that including np because of the larger radiative decay rate nf-$3d$ [17].

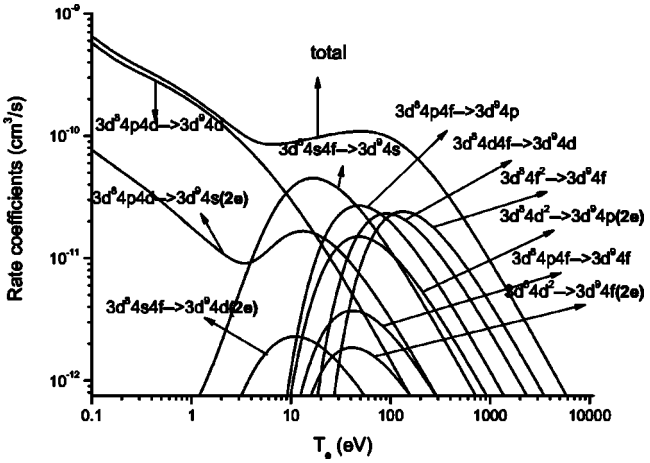

FIG. 5. State-to-state DR rate coefficient through the Pd^{18+} [Ne *core*]$3s^23p^63d^84l4l'$ as a function of electron temperature.

The state-to-state DR rate coefficients through Pd^{18+} [Ne *core*]$3s^23p^63d^84l4l'$ are displayed in Fig. 5. The rate coefficients at lower temperature come from $3d^84p4d \rightarrow 3d^94d$ transitions. As temperature increases, the $3d^84l4f \rightarrow 3d^94l$ $(l=s,p,d,f)$ become dominated and their peak positions also increase with increasing energies in the order from s to f of $3d^84l4f$ $(l=s,p,d,f)$, since energies of those doubly excited states increase in the same order. In general, the DR processes including the radiative transitions $4f \rightarrow 3d$ and $4p \rightarrow 3d$ are the dominated DR channels.

The transitions symbolized by "2*e*" denote the two-electron and one-photon transitions, which means in the transition, there is one photo emitted but two-electron orbitals change from the initial configuration to the final configuration. In the *K*-shell and *L*-shell DR processes, 2*e* transitions were thought unimportant and could be neglected [18–20]. Recently, Zou *et al.* measured this kind of two-electron and one-photon transition on the DR processes of He-like Ar^{18+} in an electron-beam ion trap (EBIT) device, and found the contribution to the total DR strength is 1.7% [23], which could be neglected in the practical applications. In the research of inertial confinement fusion, recent experiment found some unusual high-intensity two-electron and one-photon spectra of He-like and Li-like silicon in the high-density and high-temperature plasma [24,25], but it may come from the charge transfer processes instead of DR processes [24,25]. However, 2*e* transitions cannot be neglected in the present *M*-shell DR processes, such as $3d^84p4d \rightarrow 3d^9\ 4s$ and $3d^84d^2 \rightarrow 3d^94p$; their contributions are already more than 10% of the total rate coefficients, as shown in Fig. 5. In *M*-shell DR processes, there are 3 or 4 open shells in the doubly excited states. For those complicated configurations, there often exist strong configuration interactions, which induce the strong mixing of many configurations. This kind of mixing produces the 2*e* transitions. In the DR processes of Co-like Xe ions, these strong configuration interactions have been found [9]. It should be noted that the 2*e* transition may open a new DR channel, such as $3d^84d^2 \rightarrow 3d^94p$, which will increase the DR rate coefficients; otherwise, the DR processes cannot happen through the doubly excited states $3d^84d^2$. In this case, the DR rate coefficients should be increased, which is different from $3d^84p4d \rightarrow 3d^94s$. There is another main channel $3d^84p4d \rightarrow 3d^94d$, and the configuration interactions may increase or decrease the DR rate coefficients through the doubly excited states $3d^84p4d$ due to the configuration mixings. In addition, the configuration interactions also affect the energies of the doubly excited states $3d^84p4d$, and this may cause autoionization to appear or disappear for the levels close to autoionization threshold.

The state-to-state DR rate coefficients through Pd^{18+} [Ne *core*]$3s^23p^63d^84l5l'$ are plotted in Fig. 6, and only some larger DR processes are displayed. The peak positions of DR rate coefficients correspond to the energies of doubly excited states. The larger contributions come from the DR processes including transitions $4f,4p,5f,5p \rightarrow 3d$, and the largest DR processes are through the transitions $3d^84f5f \rightarrow 3d^95f$, as shown in Fig. 6. For the DR processes through $3d^84l5l'$, 2*e* transitions are not as important as that through $3d^84l4l'$, which means the configuration interactions decrease with increasing n in the doubly excited states $3d^84lnl'$.

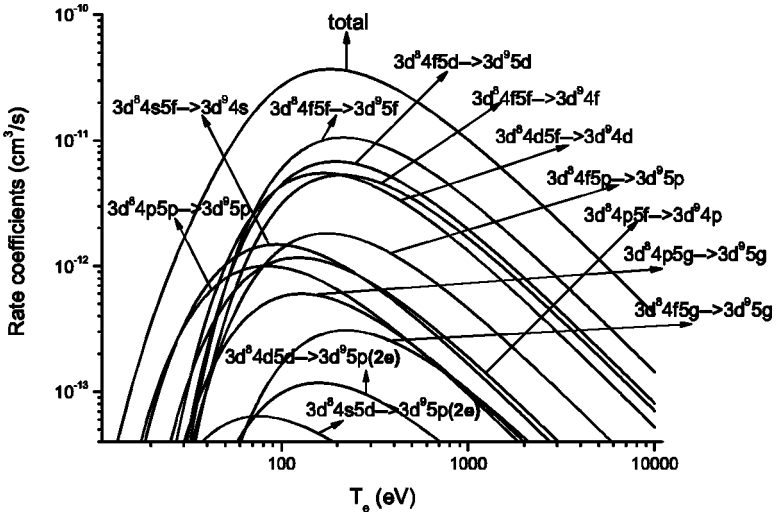

FIG. 6. State-to-state DR rate coefficient through the Pd^{18+} [Ne *core*]$3s^23p^63d^84l5l'$ as a function of electron temperature.

IV. SUMMARY

Ab initio calculations of dielectronic recombination processes from the ground state of Co-like Pd ion through the Ni-like [Ne *core*]$3s^2 3p^6 3d^8 4lnl'$, [Ne *core*]$3s^2 3p^5 3d^9 4lnl'$, [Ne *core*]$3s 3p^6 3d^9 4lnl'$ ($n=4$ or 5) are performed using the Hartree-Fock with relativistic correction method. Total and state-to-state rate coefficients are obtained in the temperature range from 0.1 to 10^4 eV. Comparison of the rate coefficients from 3*s*, 3*p*, and 3*d* subshell excitations shows 3*d* excitation dominates over the others in the whole energy region, but 3*p* and 3*s* subshell excitation cannot be neglected in high temperature. The two-electron radiative transitions, such as $3d^8 4d^2$-$3d^9 4p$ and $3d^8 4f^2$-$3d^9 4p$, are found to be important due to the strong configuration interactions. The contributions of high Rydberg doubly excited states $4lnl'$ ($n>5$) to the total rate coefficients are expected to be important. As a test, further theoretical calculations and experimental measurements are required.

ACKNOWLEDGMENTS

This work was supported by National Natural Science Foundation of China (Grant Nos. 10344001 and 10174009), Science and Technology Foundation of Chinese Academy of Engineering Physics, and National High-Tech ICF Committee in China.

[1] A. Burgess, Astrophys. J. **139**, 776 (1964).
[2] A. V. Vinogradov, I. Yu. Skobelev, and E. A. Yukov, Zh. Eksp. Teor. Fiz. **72**, 1762 (1977) [Sov. Phys. JETP **45**, 925 (1977)].
[3] J. Dubau, A. H. Gabriel, M. Loulergue, L. Steenman-Clark, and S. Volonte, Mon. Not. R. Astron. Soc. **195**, 705 (1981).
[4] J. Dubau and S. Volonte, Rep. Prog. Phys. **43**, 199 (1980).
[5] E. Behar, P. Mandelbaum, J. L. Schwob, A. Bar-Shalom, J. Oreg, and W. H. Goldstein, Phys. Rev. A **52**, 3770 (1995).
[6] E. Behar, P. Mandelbaum, J. L. Schwob, A. Bar-Shalom, J. Oreg, and W. H. Goldstein, Phys. Rev. A **54**, 3070 (1996).
[7] R. Doron *et al.*, J. Quant. Spectrosc. Radiat. Transf. **71**, 305 (2001).
[8] J. Yan, P. Li, C. L. Liu, Y. B. Qiu, and Q. Y. Fang, Chin. Phys. **19**, 1124 (2001).
[9] J. Yan, Y.-M. Li, and J.-H. Yao, Nucl. Instrum. Methods Phys. Res. B **205**, 382 (2003).
[10] J. P. Apruzese, J. Davis, M. Blaha, P. C. Kepple, and V. L. Jacobs, Phys. Rev. Lett. **55**, 1877 (1985).
[11] H. M. Peng *et al.*, *X-ray Laser* (National Defence Press, Beijing, 1997).
[12] A. Sasaki and T. Kawachi, J. Quant. Spectrosc. Radiat. Transf. **81**, 411 (2003).
[13] J. G. Wang, Y. Zou, and T. Q. Chang, Acta Phys. Sin. **46**, 2146 (1997).
[14] P. J. Gu, J. G. Wang, and T. Q. Chang, High Power Lasers and Particle Beams **11**, 78 (1999).
[15] M. E. Foord, S. H. Glenzer, R. S. Thoe, K. L. Wong, K. B. Fournier, B. G. Wilson, and P. T. Springer, Phys. Rev. Lett. **85**, 992 (2000).
[16] M. Primout *et al.*, J. Quant. Spectrosc. Radiat. Transf. **71**, 331 (2001).
[17] R. D. Cowan, *The Theory of Atomic Structure and Spectra* (University of California Press, Berkeley, CA, 1981).
[18] J. G. Wang, Y. Z. Qu, and J. M. Li, Phys. Rev. A **52**, 4274 (1995).
[19] Y. Z. Qu, J. G. Wang, J. K. Yuan, and J. M. Li, Phys. Rev. A **57**, 1033 (1998).
[20] J. G. Wang, T. Kato, and I. Murakami, Phys. Rev. A **60**, 2104 (1999).
[21] M. H. Chen, Phys. Rev. A **33**, 994 (1986).
[22] K. R. Karim and C. P. Bhalla, Phys. Rev. A **37**, 2599 (1988).
[23] Y. Zou, J. R. Crespolopez-Urrutia, and J. Ullrich, Phys. Rev. A **67**, 042703 (2003).
[24] R. C. Elton *et al.*, J. Quant. Spectrosc. Radiat. Transf. **65**, 185 (2000).
[25] F. B. Rosmej *et al.*, Phys. Rev. E **66**, 056402 (2002).